J Stat Phys (2007) 128: 1391–1414
DOI 10.1007/s10955-007-9346-5

Analysis of Path Integrals at Low Temperature: Box Formula, Occupation Time and Ergodic Approximation

Sébastien Paulin · Angel Alastuey · Thierry Dauxois

Received: 27 July 2006 / Accepted: 9 May 2007 / Published online: 3 July 2007

Abstract We study the low temperature behavior of path integrals for a simple one-dimensional model. Starting from the Feynman–Kac formula, we derive a new functional representation of the density matrix at finite temperature, in terms of the occupation times for Brownian motions constrained to stay within boxes with finite sizes. From that representation, we infer a kind of ergodic approximation, which only involves double ordinary integrals. As shown by its applications to different potentials, the ergodic approximation turns out to be quite efficient, especially in the low-temperature regime where other usual approximations fail.

1 Introduction

The knowledge of the density matrix at finite temperature T for few interacting particles, is important for studying equilibrium properties of quantum many-body systems. In this context, the Feynman–Kac (FK) representation of the density matrix in terms of path integrals [1–4] is particularly useful. On the one hand, it has been used for deriving exact analytical expressions for simple models (see e.g. [5]). On the other hand, beyond the well-known Wigner-Kirkwood expansion [6–9] around the classical limit, various approximations, non-perturbative in $\hbar$, have been introduced within that framework: for instance, the celebrated semi-classical approximation [1, 11] or the variational approach of Feynman and Kleinert [10].

The FK representation is described in Sect. 2. For the sake of pedagogy, we consider a single particle in one dimension submitted to a stationary potential. Furthermore, the infimum of the corresponding spectrum is assumed to be a bound state. The mean spatial extension of the Brownian paths, which intervene in the FK representation, is controlled by the thermal de Broglie wavelength of the quantum particle. At high temperatures, Wigner–

S. Paulin · A. Alastuey · T. Dauxois (✉)
Laboratoire de Physique, CNRS, ENS Lyon, 46 allée d'Italie, 69364 Lyon cédex 07, France
e-mail: Thierry.Dauxois@ens-lyon.fr

Kirkwood $\hbar^2$-expansions around the classical limit, which have been derived long ago in other frameworks, are easily recovered since path extension vanishes. At finite temperatures, non-perturbative effects in $\hbar$ can be accounted for through various approximations [10, 11], which are briefly described. When temperature goes to zero, the asymptotic structure of the density matrix, provided by the groundstate contribution in its spectral expression, does not clearly emerge from its FK representation. In fact, in that temperature regime, the average extension of paths diverge, whereas the main contribution to the functional integral arises from paths with a finite extension, of the order of the localization length of the ground state: contributions of such minority paths are significantly different from the average contribution. Most of our knowledge is negative, i.e. tells us which trajectories are not important [12], so, in some sense, we will try to have a positive attitude [13].

In this paper, we derive a new functional representation of the density matrix, which is more suitable than the genuine FK formula for tackling the low-temperature regime (see Sect. 3). The starting central observations are described in Sect. 3.1. First, in the FK functional integral, only marginal paths with finite extensions, i.e. large deviations with respect to the average, contribute when T goes to zero. Second, many of such paths with quite different jagged shapes, provide similar contributions, mainly determined by the corresponding local occupation times. Thus, it is quite natural to collect paths into sets defined by their spatial extension and their local occupation times. That procedure allows us to transform exactly FK representation (2) into the so-called box formula (13). That formula is defined *via* the introduction of paths constrained to stay in a box with size ℓ and characterized by an intermediate flight time s (in $\beta\hbar$ units with $\beta = 1/k_B T$). It involves a double ordinary integral over ℓ and s, combined to functional integrals over local occupation times associated with the constrained paths. As required, box formula (13) provides a better understanding of the low-temperature behavior of the density matrix than FK representation (2). When T vanishes, leading contributions obviously arise from typical sizes ℓ much smaller than de Broglie wavelength. In a forthcoming paper, we will argue how groundstate quantities emerge from box formula (13), by using scaling properties of the probability distribution function (PDF) of occupation times at low temperatures.

Beyond its conceptual interest for understanding low-temperature behaviors of path integrals, box formula (13) also allows us to derive new approximations. This is illustrated in Sect. 4, where we present the so-called ergodic approximation. That approximation results from the truncation to first order of cumulant expansions of the functional averages. It amounts to replace each local occupation time associated with a given constrained path, by its average over the corresponding PDF. This can be viewed as some kind of ergodic hypothesis, because the imaginary-time average of the potential experienced by the particle along that path, is then replaced by a spatial average with a measure defined by the mean occupation-time. Ergodic expression (16) involves only an ordinary double integral over ℓ and s, so the tremendous difficulty of computing a functional integral is circumvented. The key ingredient, namely the mean occupation-time (in units of $1/\ell$), depends on three dimensionless variables. Using its low and high temperature behaviors derived analytically, we propose simple tractable expressions for that quantity, which turn out to be quite accurate at any temperature.

Section 5 is devoted to the applications of the ergodic approximation to various simple forms of the potential. First, we determine the asymptotic analytical forms of the approximate density matrices at both low and high temperatures. When T diverges, Wigner–Kirkwood expansion is partially recovered. When T vanishes, the main features of the exact behaviors are well reproduced. The approximate density matrices then do factorize as a

product of a Boltzmann factor associated with a given energy, times a function of position only: this provides satisfactory approximate expressions for the groundstate energy and wavefunction. Second, numerical calculations are performed at finite intermediate temperatures. As expected from the previous analytical results, the ergodic approximation turns out to be quite reasonably accurate over the whole range of considered temperatures, and discrepancies with numerically exact results[1] do not exceed a few percent in most cases. Moreover, it significantly improves over the well-known semi-classical approximation, in particular at low temperatures (except for the harmonic potential of course). Also, further applications and extensions of the ergodic approximation to other potentials and two- or three-dimensional systems with one or two particles, are briefly discussed.

Let us mention that various computationally exact methods have been derived for calculating path integrals with an arbitrary high accuracy. A first type of such methods starts with Trotter formula, and rely on the use of simple thermal propagators (see e.g. [14]), combined to Monte Carlo sampling of multi-dimensional integrals and other algorithmic tricks [15, 16]. Quantum Monte Carlo methods extend those approaches to many-body systems, for which they have provided remarkable results (see e.g. [16–18]). Another type of computationally exact methods follows from Ito–Nisio theorem [19] and involve decompositions of Brownian paths on suitable basis.

Eventually, we emphasize that our approach is not intended to provide numerically exact results. The ergodic formula (16) enters in the class of simple approximation schemes, like those described above [10, 11], which account for non-perturbative quantum effects. Its main advantages rely on both an analytical control of low-temperature behaviors, and an accurate description over a wide temperature-range *via* numerical calculations easily performed by a pocket calculator. In the framework of the many-body problem, this should be useful for various purposes, like fast and reliable estimates of first quantum virial coefficients in low-fugacity expansions, or tractable modelizations of two-body effective interactions. Also, use of the ergodic approximation for few-body density matrices in quantum Monte Carlo methods, might improve the accuracy and convergence of the corresponding calculations.

2 Path Integral Framework

In this Section, we first define the model and then introduce the FK representation of the corresponding density matrix. Next, we briefly recall the efficiency of FK formula for describing the high-temperature regime, and we argue about its drawbacks for analyzing low-temperature behaviors.

We consider a quantum non-relativistic particle of mass m in one dimension z with Hamiltonian $H = -\hbar^2/(2m)\Delta + V(z)$. The matrix elements of Gibbs operator $\rho = \exp[-\beta H]$ with $\beta = 1/(k_B T)$, define the so-called density matrix $\rho(x, y, \beta) = \langle x|\rho|y\rangle$. The partition function $Z(\beta) = \mathrm{Trace}[\rho]$ is well behaved for a confining potential such that $V(z) \to \infty$ when $|z| \to \infty$. The normalized probability density to find the particle at position x then reduces to $\Psi(x, \beta) = \rho(x, x, \beta)/Z(\beta)$. For a potential which vanishes at infinity in an integrable way, we introduce the virial coefficient $B(\beta) = \mathrm{Trace}[\rho - \rho_0]$ where ρ_0 is the free density matrix, as well as the normalized deviation to the uniform free density

[1] Such results are inferred from the spectral representation on the one hand, and from a transfer-matrix diagonalization method specific to one-dimensional systems on the other hand.

$\Phi(x,\beta) = [\rho(x,x,\beta) - \rho_0(x,x,\beta)]/B(\beta)$.[2] For further purposes, it is also convenient to introduce the spectral representation of the density matrix

$$\rho(x,y,\beta) = \sum_{k=0}^{+\infty} \phi_k(x)\phi_k^*(y)\exp(-\beta E_k), \tag{1}$$

where ϕ_k is the k-th eigenstate of H with energy E_k. It is understood that, for the continuous part of the spectrum, the discrete sum in the r.h.s. of (1) is replaced by an integral over the energies of diffusion states.

Path integrals were first introduced for representing the matrix elements of the evolution operator $\exp(-iHt/\hbar)$ associated with Schrödinger equation [1]. It was soon realized that a similar path integral representation for matrix elements of Gibbs operator at inverse temperature β can be inferred *via* the formal substitution $t \to -i\beta\hbar$. In that genuine representation of $\rho(x,y,\beta)$, paths can be rewritten within the parametrization $\omega(u) = (1-s)x + sy + \lambda_D\xi(s)$, where $s = u/(\beta\hbar)$ is the dimensionless time in $\beta\hbar$ units, while $\xi(s)$ is a Brownian bridge satisfying boundary conditions $\xi(0) = \xi(1) = 0$ and $\lambda_D = (\beta\hbar^2/m)^{1/2}$ is the de Broglie wavelength. This provides the so-called Feynman–Kac formula [2–4]

$$\rho(x,y,\beta) = \frac{\exp[-(x-y)^2/(2\lambda_D^2)]}{\sqrt{2\pi}\lambda_D} \times \int_\Omega \mathcal{D}_W(\xi)\exp\left(-\beta\int_0^1 \mathrm{d}s\, V((1-s)x + sy + \lambda_D\xi(s))\right) \tag{2}$$

where $\Omega = \{\xi(\cdot)\}$ is the infinite set of realizations of the Brownian bridge process, while $\mathcal{D}_W(\xi)$ is the normalized Gaussian Wiener measure defined by its first two moments, $\langle\xi(s)\rangle_\Omega = 0$ and $\langle\xi(s_1)\xi(s_2)\rangle_\Omega = \min(s_1,s_2)(1-\max(s_1,s_2))$. Wiener measure is intrinsic to Brownian motion and does not depend on any physical parameter. Mass m of the particle, as well as Planck's constant $\hbar$ only intervene in the de Broglie wavelength λ_D, which controls the size of quantum fluctuations, as shown by specifying (2) to diagonal elements, i.e.

$$\rho(x,x,\beta) = \frac{1}{\sqrt{2\pi}\lambda_D}\int_\Omega \mathcal{D}_W(\xi)\exp\left(-\beta\int_0^1 \mathrm{d}s\, V(x+\lambda_D\xi(s))\right). \tag{3}$$

In time-average $\int_0^1 \mathrm{d}s\, V(x+\lambda_D\xi(s))$, particle experiences the potential around position x on a length scale obviously determined by λ_D, as illustrated in Fig. 1. Notice that, besides its interest for analytical or numerical calculations (see below), Feynman–Kac representation is also quite useful for mapping a quantum system into a classical one [20–23].

At high temperatures, de Broglie wavelength is small, so only paths which remain close to reference position x contribute significantly to $\rho(x,x,\beta)$ in (3). Therefore, the time-average of V along path $x+\lambda_D\xi(s)$ can be performed by replacing $V(x+\lambda_D\xi(s))$ by its Taylor series around $V(x)$. This generates quantum corrections to classical form $\exp[-\beta V(x)]/(\sqrt{2\pi}\lambda_D)$ because λ_D is proportional to $\hbar$. Thanks to Wick's theorem, we

[2] Virial coefficient B occurs in low-fugacity expansions of thermodynamical quantities for a many-body system made with two-body interactions $V(x_i - x_j)$. Deviation Φ then determines leading particle correlations at low densities.

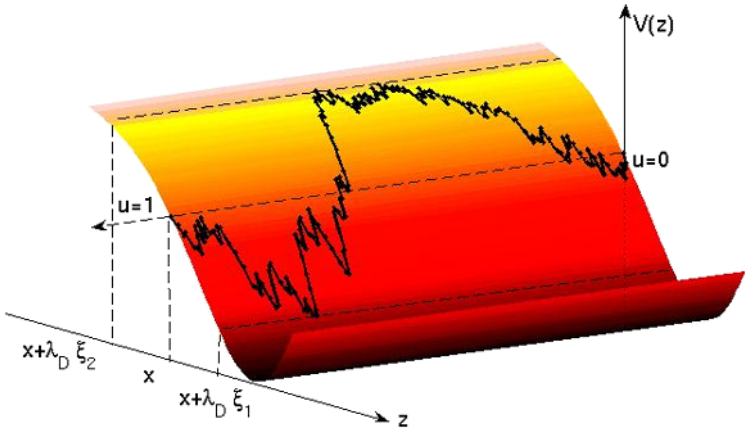

Fig. 1 (Color online) Typical path which starts and ends at position x, along which particle experiences potential V. *Dashed lines* indicate the two edges of a fictitious box determined by the extremal deviations ξ_1 and ξ_2 of the path. Typical sizes of ξ_1 and ξ_2 are of order one

easily retrieve the well-known Wigner–Kirkwood expansion in powers of $\hbar^2$

$$\rho(x,x,\beta)=\frac{e^{-\beta V(x)}}{\sqrt{2\pi}\lambda_D}\left[1-\frac{\beta^2\hbar^2}{12m}\frac{\mathrm{d}^2V}{\mathrm{d}x^2}+\frac{\beta^3\hbar^2}{24m}\left(\frac{\mathrm{d}V}{\mathrm{d}x}\right)^2+\cdots\right], \tag{4}$$

which was derived long ago by using the Wigner-distribution formalism (see e.g. Ref. [9]). Previous method might be used for calculating higher-order terms beyond $\hbar^2$-correction (terms up to order $\hbar^6$ have been already determined in the literature [24]). Moreover, it clearly emphasizes that expansion (4) is appropriate when the de Broglie wavelength is much smaller than the typical length of variation of the potential.

When the temperature decreases, the de Broglie wavelength increases, so Wigner–Kirkwood expansion is no longer applicable. At the analytical level, exact evaluations of the corresponding path integrals are not accessible in general, except for some simple models [5]. Non-perturbative effects in $\hbar$ can be partially accounted for through various methods. The celebrated semi-classical approximation is based on an expansion with respect to the deviation of an arbitrary path with respect to the classical trajectory. The truncation of that expansion up to second order leads to a Gaussian functional integral, which is exactly computed in terms of the classical action and its derivatives [11]. A second method relies on the introduction of auxiliary harmonic potentials with adjustable frequencies [10]. Such frequencies are then determined by a variational criterion which follows from Jensen inequality. The reliability of those methods remains questionable since they do not involve any small control-parameter like (4). Nonetheless, for numerical purposes, their accuracy may be satisfactory, at least at not too low temperatures.

When temperature goes to zero, λ_D diverges, so most paths explore a rather large region not restricted to the neighborhood of reference position x. A direct analysis of FK expression (3) then becomes quite cumbersome. In particular, $\rho(x,x,\beta)$ must behave as

$$\rho(x,x,\beta)\overset{\beta\to+\infty}{\sim}|\phi_0(x)|^2\exp[-\beta E_0], \tag{5}$$

which immediately follows from spectral representation of density matrix (1). The factorization of position and temperature dependencies in (5) does not come out easily from FK

formula (3), where both position and temperature are coupled in an absolutely non-trivial way.

3 Box Formula

3.1 The Central Observations

For fixing ideas, let us consider a symmetric potential $V(z)$ with a minimum located at $z = 0$. On the one hand, low-temperature behavior (5) of the corresponding density matrix is mainly determined by the local shape of $V(z)$ over finite length scale a_0, which characterizes the spatial extension of the groundstate wave function $\phi_0(x)$. On the other hand, for typical paths with size of order λ_D, time-average potential $\int_0^1 \mathrm{d}s\, V(x + \lambda_D \xi(s))$ becomes, roughly speaking, of order $\int_0^{\lambda_D} \mathrm{d}z\, V(z)/\lambda_D$ when λ_D is sufficiently large. At low temperatures, $\beta \int_0^1 \mathrm{d}s\, V(x + \lambda_D \xi(s))$ does not behave as a constant times β in general. Thus, low-temperature behavior (5) is not provided by typical paths. That argument can be implemented through semi-quantitative estimations in some specific cases. For a confining potential which diverges as $|z|^n$ $(n > 0)$, contributions of typical paths to (3) then behave (discarding multiplicative powers of β) as $\exp(-c\beta^{1+n/2})$ with some positive constant c. For integrable potentials, such contributions become of order $\exp(-c/\beta^{1/2})$. In both cases, typical contributions are exponentially smaller than leading Boltzmann factor $\exp[-\beta E_0]$.

The previous analysis suggests that, at low temperatures, leading contributions to the r.h.s. of (3) arise from paths with a spatial extension of order a_0, i.e. from quite small Brownian bridges with size $|\xi(s)|$ of order a_0/λ_D. For such paths, time-average potential $\int_0^1 \mathrm{d}s\, V(x + \lambda_D \xi(s))$ is of order $V(a_0)$, so the corresponding Boltzmann factor indeed is of order $\exp[-\beta E_0]$. Notice that, paths with very different shapes give raise to similar contributions, since the Wiener weights of the associated Brownian bridges remain of order (roughly speaking) $\exp(-\int_0^1 \mathrm{d}s (\dot{\xi}(s))^2/2) \sim \exp(-a_0^2/\lambda_D^2) \sim 1$. Consequently, when the temperature decreases, only a very tiny subset of paths gives a relevant contribution to the r.h.s. of (3). In other words, important paths are not any more typical but, on the contrary, they can be viewed as large deviations. This explains why direct numerical evaluations of (3) become rather difficult: the subset of important paths remains, in some sense, hidden in the entire configurational space.

In order to extract from (3) the relevant contributions at low temperatures, it is tempting to collect all paths with the same finite spatial extension, and then to sum over all possible extensions. That procedure is not easy to carry out directly in the r.h.s. of (3), within a suitable partition of functional integration space over Brownian bridges. As described below, it is more convenient to transform first the density matrix within the operator representation, by introducing an auxiliary Hamiltonian which confines the particle inside a box with size ℓ.

3.2 The Auxiliary Hamiltonian Approach

Let us introduce the auxiliary Hamiltonian $H_\ell = H^0 + V + V_\ell$, where H^0 denotes the kinetic Hamiltonian. The additional potential V_ℓ is defined by

$$V_\ell(z) = V_0[1 - \Theta(z + \ell) + \Theta(z - l)], \tag{6}$$

where Θ is the Heavyside function, while V_0 denotes barrier height $(V_0 > 0)$. That potential tends to confine the particle inside a box with extension ℓ. The auxiliary Hamiltonian

reduces to the genuine one when ℓ goes to infinity. In that limit, for x kept fixed, diagonal part $\langle x|\rho_\ell|x\rangle$ of density matrix $\rho_\ell = \exp[-\beta H_\ell]$ goes to $\langle x|\rho|x\rangle$.

The identity,

$$\langle x|\rho|x\rangle = \langle x|\rho_L|x\rangle + \int_L^\infty \mathrm{d}\ell \langle x|\partial_\ell[\rho_\ell]|x\rangle \tag{7}$$

which is valid for any reference extension L and for any height V_0 of the confining potential is quite useful for our purpose. We set $L = |x|$, and we consider an infinitely high potential barrier V_0. Under that limit, $\langle x|\rho_L|x\rangle$ goes to zero because the probability for the particle to stay on the boundary vanishes for infinitely high walls. By using Dyson formula for $\partial_\ell[\rho_\ell]$, we then obtain

$$\begin{aligned}\rho(x,x,\beta) = \lim_{V_0\to\infty} \beta V_0 \int_{|x|}^\infty \mathrm{d}\ell \int_0^1 \mathrm{d}s [\rho_\ell(x,\ell,\beta[1-s])\rho_\ell(\ell,x,\beta s) \\ + \rho_\ell(x,-\ell,\beta[1-s])\rho_\ell(-\ell,x,\beta s)].\end{aligned} \tag{8}$$

Expression (8) must be considered with some caution because when V_0 diverges the different integrands vanishes. In order to control limit $V_0 \to \infty$, we rewrite the integrands in terms of constrained density matrix ρ_ℓ^0 of the *free* particle submitted to confining potential V_ℓ. After defining

$$g^\pm(x,\ell,s,\beta) = \lim_{V_0\to\infty} (2\pi)^{1/2}\lambda_D(\beta V_0)\rho_\ell^0(x,\pm\ell,\beta s)\rho_\ell^0(\pm\ell,x,\beta(1-s)), \tag{9}$$

we transform (8) into

$$\begin{aligned}\rho(x,x,\beta) = &\int_{|x|}^{+\infty} \mathrm{d}\ell \int_0^1 \mathrm{d}s \frac{g^-(x,\ell,s,\beta)}{\sqrt{2\pi}\lambda_D} \left\langle \exp\left[-\beta s \int_0^1 \mathrm{d}u\, V(z(u))\right]\right\rangle_{\Omega_s^-} \\ &\times \left\langle \exp\left[-\beta(1-s)\int_0^1 \mathrm{d}u\, V(z(u))\right]\right\rangle_{\Omega_{1-s}^-} \\ &+ \int_{|x|}^{+\infty} \mathrm{d}\ell \int_0^1 \mathrm{d}s \frac{g^+(x,\ell,s,\beta)}{\sqrt{2\pi}\lambda_D} \left\langle \exp\left[-\beta s \int_0^1 \mathrm{d}u\, V(z(u))\right]\right\rangle_{\Omega_s^+} \\ &\times \left\langle \exp\left[-\beta(1-s)\int_0^1 \mathrm{d}u\, V(z(u))\right]\right\rangle_{\Omega_{1-s}^+}.\end{aligned} \tag{10}$$

Notation $\langle . \rangle_\omega$ denotes an average over a constrained Brownian process which belongs to a set ω. Paths $z(u)$ are expressed in terms of Brownian bridges according to $z(u) = x(1-u) \pm u\ell + \sqrt{s}\lambda_D\xi(u)$ for $\Omega_s^\pm$. Moreover those paths must stay inside the box $[-\ell, +\ell]$, so that constraint defines the corresponding sets $\Omega_s^\pm$. The statistical weight of a path in such a constrained average is its associated Wiener measure $\mathcal{D}_W(\xi)$. For the sake of notational convenience, we do not explicitly write the dependencies on both x and ℓ of $\Omega_s^\pm$.

The physical interpretation of functions $g\pm$ clearly emerges from (10), if we specify that general formula to the particular case $V(z) = 0$. Such functions are the (normalized) statistical weights of the constrained sets $\Omega^\pm = \Omega_s^\pm \cup \Omega_{1-s}^\pm$, i.e. the sum of statistical weights of all paths touching the boundaries of the box at time s (see Fig. 2). Therefore, in the following, we set $g^\pm(x,\ell,s,\beta) = g(\Omega^\pm)$. Analytical calculations of those weights are performed in Appendix, by using the spectral representation of ρ_ℓ^0.

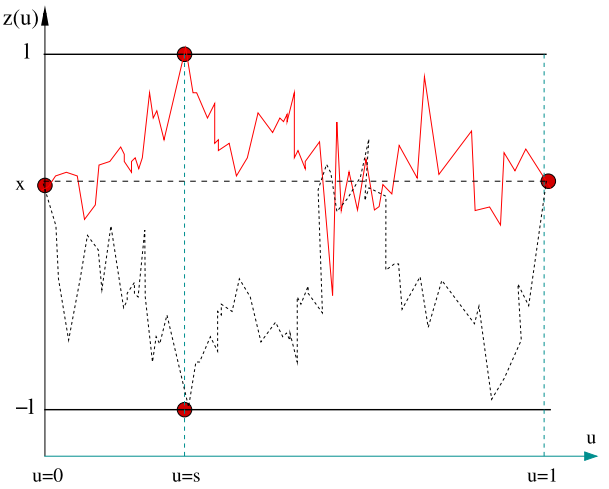

Fig. 2 (Color online) Typical paths which start and end at position x. *Solid and dashed lines* represent paths which belong to Ω^+ and to Ω^- respectively

The first step of our rewriting of Feynman–Kac representation, is achieved through formula (10). Paths are indeed collected together according to their extension $\pm\ell$. Notice that the touching time, s, is also crucial for defining the corresponding proper partition of the genuine integration space over all unconstrained paths.

3.3 Introduction of Averages Over Occupation Times

In a second step, we introduce the so-called *occupation time*, defined for each given path $z(u)$ in $\Omega_s^{\pm}$ by

$$\theta_z(x') = \int_0^1 \mathrm{d}u\,\delta(x' - z(u)). \tag{11}$$

The quantity $\theta_z(x')\mathrm{d}x'$ is the total time passed in a neighborhood $\mathrm{d}x'$ of position x' by the particle when it follows Brownian path $z(u)$. Of course, the total time passed in the whole box is always equal to 1, i.e. $\int_{-\ell}^{+\ell} \mathrm{d}x'\theta_z(x') = 1$. Time-averaged potential along path $z(u)$ is then expressed in terms of occupation time *via* the obvious identity

$$\int_0^1 \mathrm{d}u\,V(z(u)) = \int_{-\ell}^{+\ell} \mathrm{d}x'\theta_z(x')V(x'), \tag{12}$$

valid for any path $z(u)$.

According to identity (12), Boltzmann factors involved in averages $\langle\cdots\rangle_{\Omega_s^{\pm}}$ in the r.h.s. of (10), only depend on the occupation time $\theta_z(x')$. As illustrated in Fig. 3, various different paths may provide the same occupation time. As quoted in Sect. 3.1, their statistical weights are close together, so their contributions to $\langle\cdots\rangle_{\Omega_s^{\pm}}$ are almost identical. Thus, it is now tempting to collect all paths which provide the same occupation time $\theta(x')$, *via* the introduction of the corresponding density measure $\mathcal{D}_{\Omega_s^{\pm}}[\theta]$. After expressing averages over constrained paths, as averages over occupation times with (normalized) measure $\mathcal{D}_{\Omega_s^{\pm}}[\theta]$, we eventually obtain the box formula

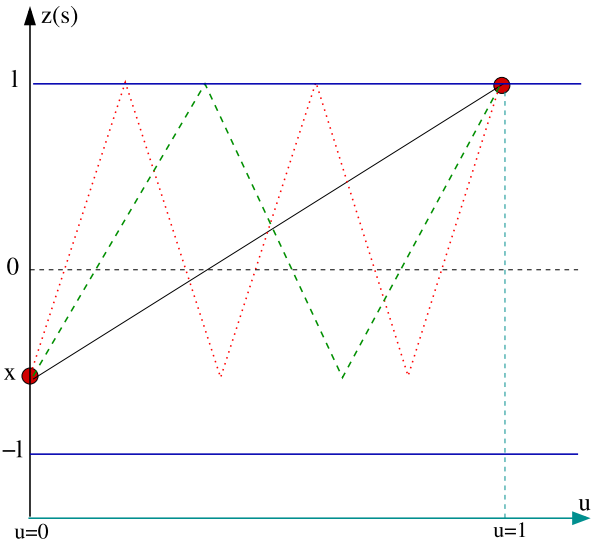

Fig. 3 (Color online) Three different paths which start at x and end at $+\ell$, while the corresponding occupation times are identical

$$\rho(x,x,\beta)=\int_{|x|}^{+\infty}\mathrm{d}\ell\int_0^1\mathrm{d}s\,\frac{g(\Omega^-)}{\sqrt{2\pi}\lambda_D}\int\mathcal{D}_{\Omega_s^-}[\theta]\exp\left[-\beta s\int_{-\ell}^{+\ell}\mathrm{d}x'\theta(x')V(x')\right]$$
$$\times\int\mathcal{D}_{\Omega_{1-s}^-}[\theta]\exp\left[-\beta(1-s)\int_{-\ell}^{+\ell}\mathrm{d}x'\theta(x')V(x')\right]$$
$$+\int_{|x|}^{+\infty}\mathrm{d}\ell\int_0^1\mathrm{d}s\,\frac{g(\Omega^+)}{\sqrt{2\pi}\lambda_D}\int\mathcal{D}_{\Omega_s^+}[\theta]\exp\left[-\beta s\int_{-\ell}^{+\ell}\mathrm{d}x'\theta(x')V(x')\right]$$
$$\times\int\mathcal{D}_{\Omega_{1-s}^+}[\theta]\exp\left[-\beta(1-s)\int_{-\ell}^{+\ell}\mathrm{d}x'\theta(x')V(x')\right]. \tag{13}$$

If statistical weights $g(\Omega^\pm)$ are analytically known (see Appendix), explicit expressions for density measures $\mathcal{D}_{\Omega_s^\pm}[\theta]$ are not available. Such probability densities result from the summation of Wiener measures over all Brownian paths inside $\Omega_s^\pm$ which provide the same occupation time. That procedure is quite difficult to handle in closed analytical forms, and only the moments of $\mathcal{D}_{\Omega_s^\pm}[\theta]$ can be computed explicitly. Nevertheless, box formula (13) turns out to be quite useful for various purposes, as suggested by the following simple comments and arguments.

Contrary to the case of the genuine Feynman–Kac representation, leading contributions at low temperature merely emerge from box formula (13). Indeed, for x of order a_0, boxes with size ℓ of order a few a_0 do provide contributions of order $\exp(-\beta E_0)$, because weight factors $g(\Omega^\pm)$ are of order $\exp(-\pi^2\lambda_D^2/(8\ell^2))$ for $\ell\ll\lambda_D$ (see Appendix), while products of averages of Boltzmann factors over occupation times are of order $\exp(-\beta\int_0^\ell\mathrm{d}x'V(x')/\ell)$. That rough analysis will be implemented in a forthcoming paper, where we show more precisely how low temperature behavior (5) arises from scaling properties of distributions $\mathcal{D}_{\Omega_s^\pm}[\theta]$ in the regime $\ell\ll\lambda_D$.

If Brownian paths are quite noisy, the corresponding occupation times may have rather regular shapes. This is illustrated in Fig. 4(a), which shows a regular path on the one hand, an a very jagged one on the other hand: both paths provide occupation times with regular shapes

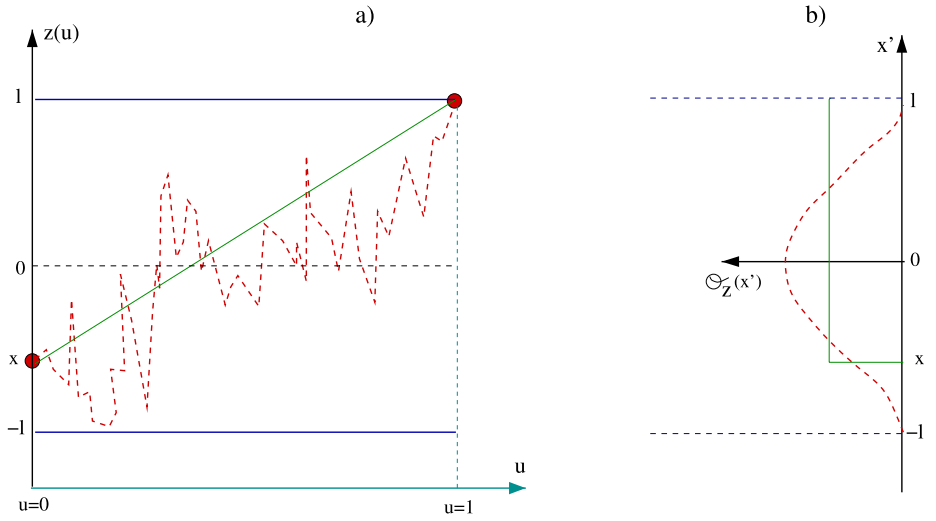

Fig. 4 (Color online) Panel (**a**) presents two different paths which start at position x at time $u = 0$ and end at ℓ for time $u = 1$. Panel (**b**) shows their corresponding occupation times $\theta_z(x')$

displayed in Fig. 4(b) (notice that the corresponding contributions to Boltzmann factors are of course different). That observation leads to a first type of approximations based on simple modelizations of distributions $\mathcal{D}_{\Omega_s^{\pm}}[\theta]$ within restricted sets of elementary functions which represent the various occupation times (they will be described elsewhere). A second type of approximations is based on the truncation of cumulant expansions, where key ingredients do exhibit regular behaviors with respect to spatial positions. One of them is presented further in Sect. 4.

4 Ergodic Approximation

4.1 Truncation of the Cumulant Expansion

Formally, averages over distributions $\mathcal{D}_{\Omega_s^{\pm}}[\theta]$ involved in the r.h.s. of box formula (13) can be represented by their infinite cumulant expansions. A natural approximation consists in truncating that expansion up to its first term, i.e. we replace the averages

$$\int \mathcal{D}_{\Omega_s^{\pm}}[\theta] \exp\left[-\beta s \int_{-\ell}^{+\ell} \mathrm{d}x' \theta(x') V(x')\right] \tag{14}$$

by

$$\exp\left(-\beta s \int_{-\ell}^{+\ell} \mathrm{d}x' \langle \theta(x') \rangle_{\Omega_s^{\pm}} V(x')\right). \tag{15}$$

We call that lowest order approximation *ergodic*, since it would be exact if paths were experiencing all parts of the potential with a probability independent of time. It amounts to replace (imaginary) time averages of the potential by spatial averages with a measure defined by mean occupation-time $\langle \theta(x') \rangle_{\Omega_s^{\pm}}$. Inserting (15) into (13), we obtain the subsequent

ergodic approximation for density matrix,

$$\rho_{\rm erg}(x,x,\beta)=\int_{|x|}^{+\infty}{\rm d}\ell\int_0^1{\rm d}s\frac{g(\Omega^-)}{\sqrt{2\pi}\lambda_D}\times\exp\left[-\beta\int_{-\ell}^{+\ell}{\rm d}x'(s\langle\theta(x')\rangle_{\Omega_s^-}+[1-s]\langle\theta(x')\rangle_{\Omega_{1-s}^-})V(x')\right]+\int_{|x|}^{+\infty}{\rm d}\ell\int_0^1{\rm d}s\frac{g(\Omega^+)}{\sqrt{2\pi}\lambda_D}\times\exp\left[-\beta\int_{-\ell}^{+\ell}{\rm d}x'(s\langle\theta(x')\rangle_{\Omega_s^+}+[1-s]\langle\theta(x')\rangle_{\Omega_{1-s}^+})V(x')\right]. \quad (16)$$

Notice that Jensen inequality ensures $\rho_{\rm erg}(x,x,\beta)\le\rho(x,x,\beta)$.

4.2 Mean Occupation Time in Terms of Brownian Green Functions

The average occupation time can be obtained within two different methods: either by using operator algebra or, in a more physical way, by using Brownian motion properties, as shown below. First we compute the mean occupation time around position x', over Brownian paths at inverse temperature β' which start from x_i at time $u=0$ and end at x_f for time $u=1$. Those Brownian paths are constrained within the interval $[-\ell,+\ell]$, and they define a set $\omega=\{z(u)=x_i(1-u)+x_fu+\lambda\xi(u)\}$ with $\lambda^2=\beta'\hbar^2/m$.

Introducing the constrained probability density $f_\omega(z,u)$ to find the Brownian particle at the position z for time u, the mean occupation time reads

$$\langle\theta(x')\rangle_\omega=\int_0^1{\rm d}uf_\omega(x',u). \quad (17)$$

The probability density $f_\omega(x',u)$ can be generated by using the Green function $G_\omega(z,t|z_0,t_0)$ of the diffusion equation, solved with Dirichlet boundary conditions $G_\omega(\pm\ell,t|z_0,t_0)=0$ and initial condition $G_\omega(z,t_0|z_0,t_0)=\delta(z-z_0)$. That Green function reduces to

$$G_\omega(z,t|z_0,t_0)=\frac{1}{\ell}\sum_{n=1}^{\infty}\psi_n(z_0/\ell)\psi_n(z/\ell)\exp\left[-(t-t_0)\frac{\lambda^2}{\ell^2}\frac{\pi^2}{8}n^2\right], \quad (18)$$

with $\psi_n(z/\ell)=\sin[n\pi(z+\ell)/(2\ell)]$. Since Brownian motion is a Markov process, the constrained probability density $f_\omega(x',u)$ is then

$$f_\omega(x',u)=\frac{G_\omega(x',u|x_i,0)G_\omega(x_f,1-u|x',0)}{G_\omega(x_f,1|x_i,0)}. \quad (19)$$

Using scaling and symmetry properties of the Green function, we obtain

$$\langle\theta(x')\rangle_{\Omega_s^\mp}=\frac{1}{\ell}\Phi\left(\pm\frac{x}{\ell},\pm\frac{x'}{\ell},\frac{\lambda_D\sqrt{s}}{\ell}\right), \quad (20)$$

where Φ is a dimensionless function derived by using expressions (17), (18) and (19) (see below). Inserting those expressions of mean occupation times for various sets $\Omega_s^\pm$ into (16),

the ergodic form of the density matrix is rewritten as

$$\begin{aligned}
&\rho_{\mathrm{erg}}(x,x,\beta)\\
&\quad=\int_{|x|}^{+\infty}\mathrm{d}\ell\int_0^1\mathrm{d}s\,\frac{g(\Omega_s^-)}{\sqrt{2\pi}\lambda_D}\exp\left(-\beta s\int_{-1}^{+1}\mathrm{d}\alpha'\Phi\left(\frac{x}{\ell},\alpha',\frac{\pi\lambda_D\sqrt{s}}{2\ell}\right)V(\alpha'\ell)\right)\\
&\qquad\times\exp\left(-\beta[1-s]\int_{-1}^{+1}\mathrm{d}\alpha'\Phi\left(\frac{x}{\ell},\alpha',\frac{\pi\lambda_D\sqrt{1-s}}{2\ell}\right)V(\alpha'\ell)\right)\\
&\qquad+\int_{|x|}^{+\infty}\mathrm{d}\ell\int_0^1\mathrm{d}s\,\frac{g(\Omega_s^+)}{\sqrt{2\pi}\lambda_D}\exp\left(-\beta s\int_{-1}^{+1}\mathrm{d}\alpha'\Phi\left(-\frac{x}{\ell},\alpha',\frac{\pi\lambda_D\sqrt{s}}{2\ell}\right)V(-\alpha'\ell)\right)\\
&\qquad\times\exp\left(-\beta[1-s]\int_{-1}^{+1}\mathrm{d}\alpha'\Phi\left(-\frac{x}{\ell},\alpha',\frac{\pi\lambda_D\sqrt{1-s}}{2\ell}\right)V(-\alpha'\ell)\right)
\end{aligned}\tag{21}$$

with $g(\Omega_s^{\mp})=g(\pm x,\ell,s,\beta)$. In (21), all quantities are explicitly known in terms of simple series involving Gaussian and trigonometric functions. Box weight $g(x,\ell,s,\beta)$ is computed in Appendix, while a similar expression is derived for Φ in the next subsection (see formula (22)). Within the ergodic approximation, we are left with the evaluation of two ordinary integrals, which is of course much easier than a direct evaluation of the genuine functional integrals.

4.3 Analytical Estimations for Φ at Low and High Temperatures

Use of simple summation formulas [25] provides the general form

$$\Phi(\alpha,\alpha',y)=\frac{\sum_{n=1}^{\infty}\exp[-\frac{y^2}{2}n^2]\psi_n(\alpha')[n\psi_n(\alpha)\psi_n(\alpha')+\frac{2}{y^2}A_n(\alpha,\alpha')]}{\sum_{n=1}^{\infty}\psi_n(\alpha)n\exp[-\frac{y^2}{2}n^2]},\tag{22}$$

with

$$\begin{aligned}
A_n(\alpha,\alpha')=\frac{\pi}{8}\Bigg[&(1-\alpha-2\alpha')\sin\left[n\frac{\pi}{2}(\alpha+\alpha'+2)\right]\\
&+\left(1+\alpha-2\alpha'-2\frac{\alpha-\alpha'}{|\alpha-\alpha'|}\right)\sin\left[n\frac{\pi}{2}(\alpha-\alpha')\right]\Bigg].
\end{aligned}\tag{23}$$

In formula (21), third variable y of the function Φ is proportional to λ_D/ℓ. Thus the low and high temperature regimes correspond to the limits $y\to\infty$ and $y\to 0$ respectively. In the following, we derive asymptotic formulas for Φ in those two limits.

The asymptotic form of Φ when $y\to\infty$ is obtained by keeping only terms $n=1$ in formula (22). This leads to

$$\begin{aligned}
\Phi(\alpha,\alpha',y)=&\cos^2\left(\frac{\pi\alpha'}{2}\right)\left[1+\frac{\pi}{4y^2}(\alpha'-1)\tan\left(\frac{\pi}{2}\alpha'\right)\right]\\
&+\cos^2\left(\frac{\pi\alpha'}{2}\right)\left[(M_{\alpha,\alpha'}-1)\tan\left(\frac{\pi}{2}M_{\alpha,\alpha'}\right)\right.\\
&\left.+(1+m_{\alpha,\alpha'})\tan\left(\frac{\pi}{2}m_{\alpha,\alpha'}\right)\right]\frac{\pi}{4y^2}\\
&+O(\exp[-y^2/2]),
\end{aligned}\tag{24}$$

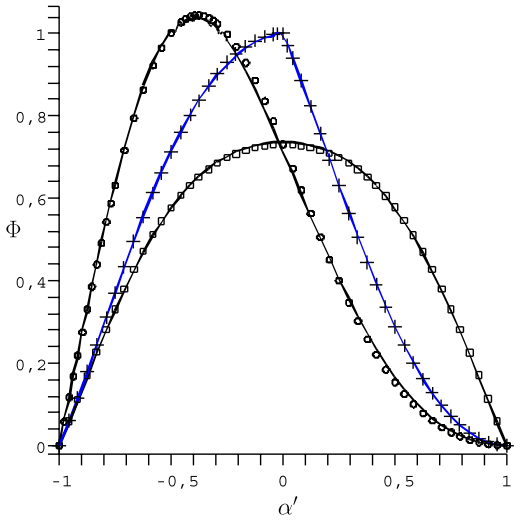

Fig. 5 (Color online) Dimensionless function $\Phi(\alpha,\alpha',2)$ for $\alpha=-0.99$ (*circles*), $\alpha=0$ (*plus signs*) and $\alpha=0.99$ (*squares*). Solid lines follow from the numerical calculation of expression (22), while points correspond to asymptotic formula (24)

where $m_{\alpha,\alpha'}=\min(\alpha,\alpha')$ and $M_{\alpha,\alpha'}=\max(\alpha,\alpha')$. Notice that the leading the term is normalized to unity (in other words, the leading term satisfies the normalization condition of Φ). Figure 5 shows the comparison between asymptotic expression (24) and the exact formula (22) evaluated numerically. Asymptotic formula is really accurate for any α, even for y close to unity.

In order to obtain the small-y behavior of Φ, the Poisson transform (46) is applied to (22). We find

$$\begin{aligned}\Phi(\alpha,\alpha',y)=\frac{1}{2}+\frac{1}{2}&\frac{(1-\alpha)+(1-\alpha)\sum_{n\neq0}\exp[-\frac{\pi^2}{y^2}n(2n-\alpha-1)]}{(1+\alpha)+\sum_{n\neq0}(1+\alpha+4n)\exp[-\frac{\pi^2}{y^2}n(1+\alpha+2n)]}\\&+\frac{\sum_{n\neq0}n\exp[-\frac{\pi^2}{2y^2}(\alpha'+\alpha-2n)(\alpha'-1-2n)]}{(1+\alpha)+\sum_{n\neq0}(1+\alpha+4n)\exp[-\frac{\pi^2}{y^2}n(1+\alpha+2n)]}\\&-\frac{\sum_{n\neq0}n\exp[-\frac{\pi^2}{2y^2}(\alpha'-\alpha-2n)(1+\alpha'-2n)]}{(1+\alpha)+\sum_{n\neq0}(1+\alpha+4n)\exp[-\frac{\pi^2}{y^2}n(1+\alpha+2n)]}\end{aligned}\tag{25}$$

for $\alpha'<\alpha$, while

$$\begin{aligned}\Phi(\alpha,\alpha',y)=\frac{1}{2}-\frac{1}{2}&\left\{(1+\alpha)-2\exp\left[-\frac{\pi^2}{2y^2}(\alpha'-\alpha)(1+\alpha')\right]\right.\\&\left.+(1+\alpha)\sum_{n\neq0}\exp\left[-\frac{\pi^2}{y^2}n(2n-\alpha-1)\right]\right\}\\&\times\left\{(1+\alpha)+\sum_{n\neq0}(1+\alpha+4n)\exp\left[-\frac{\pi^2}{y^2}n(1+\alpha+2n)\right]\right\}^{-1}\end{aligned}$$

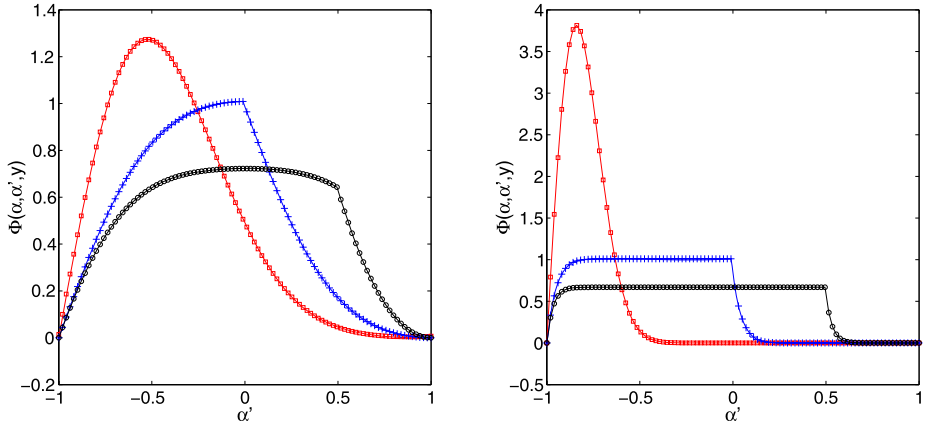

Fig. 6 (Color online) Dimensionless function $\Phi(\alpha,\alpha',1.5)$ (*left panel*) and $\Phi(\alpha,\alpha',0.5)$ (*right panel*) for $\alpha=-0.99$ (*square*), $\alpha=0$ (*cross*) and $\alpha=0.5$ (*circle*). The *solid lines* follow from numerical calculations of formulas (25–26), while symbols correspond to small-y asymptotic formula

$$+\frac{\sum_{n\neq 0} n\exp[-\frac{\pi^2}{2y^2}(\alpha'+\alpha-2n)(\alpha'-1-2n)]}{(1+\alpha)+\sum_{n\neq 0}(1+\alpha+4n)\exp[-\frac{\pi^2}{y^2}n(1+\alpha+2n)]}$$

$$+\frac{\sum_{n\neq 0}(1-n)\exp[-\frac{\pi^2}{2y^2}(\alpha'-\alpha-2n)(1+\alpha'-2n)]}{(1+\alpha)+\sum_{n\neq 0}(1+\alpha+4n)\exp[-\frac{\pi^2}{y^2}n(1+\alpha+2n)]} \qquad (26)$$

for $\alpha'>\alpha$. For y small, numerical estimates of those expressions are obtained by truncating all sums to terms $n=\pm 1$. They are compared with exact formulas (25–26) in Fig. 6 and are quite accurate for any α, and even for y close to unity. In the very high temperature regime and for almost all values of α, Φ is close to $\Theta(\alpha-\alpha')/(1+\alpha)$.

5 Applications of the Ergodic Approximation to Symmetric and Monotonic Potentials

In the remainder of the paper, we will restrict ourselves to a potential such that $V(-x)=V(x)$, $V'(x)\geq 0$ for $x\geq 0$, and either $V(x)\to\infty$ or $V(x)\to 0^-$ when $x\to\infty$. Let us focus at first on the following question: does the ergodic approximation lead to reliable estimates in the low temperature regime?

5.1 Low Temperature Regime

Inserting the asymptotic expressions (24) and (45) for Φ and g respectively into formula (21), we find the low-temperature behavior of the ergodic density matrix,

$$\rho_{\rm erg}(x,x,\beta)\overset{\beta\to\infty}{\sim}\int_{|x|}^{+\infty}\mathrm{d}\ell\,\frac{\pi^2\lambda_D^2}{8\ell^4}\sin^2\left[\frac{\pi(x+\ell)}{2\ell}\right]\exp[-\beta E(\ell)]$$
$$\times\left(\exp[-\varphi^+(\ell,x/\ell)]+\exp[-\varphi^-(\ell,-x/\ell)]\right), \qquad (27)$$

with

$$E(\ell) = \frac{\pi^2\hbar^2}{8m\ell^2} + \int_{-1}^{+1} \mathrm{d}\alpha' \cos^2\left(\frac{\pi\alpha'}{2}\right) V(\alpha'\ell), \tag{28}$$

$$\begin{aligned}\varphi^{\pm}(\ell,\alpha) = {} & \frac{2m\ell^2}{\pi\hbar^2}\left[2\int_0^1 \mathrm{d}\alpha' V(\alpha'\ell)\sin(\pi\alpha')\alpha' - \int_\alpha^1 \mathrm{d}\alpha' V(\alpha'\ell)\sin(\pi\alpha')\right] \\ & + \frac{2m\ell^2}{\pi\hbar^2}\alpha\tan\left(\frac{\pi\alpha}{2}\right) \\ & \times\left[\int_0^1 \mathrm{d}\alpha' V(\alpha'\ell)\cos^2\left(\frac{\pi\alpha'}{2}\right) - \frac{1}{\alpha}\int_0^\alpha \mathrm{d}z V(\alpha'\ell)\cos^2\left(\frac{\pi\alpha'}{2}\right)\right].\end{aligned} \tag{29}$$

Positivity of $\varphi^{\pm}$ enforces the convergence of the integral in the r.h.s. of (27) (contributions from boxes with large sizes ℓ do vanish in an integrable way). Expression (27) can still be simplified in the low temperature regime ($\beta \to \infty$), by using the saddle point method. Either the divergence of potential $V(z)$ for z large, or $\int_{-\infty}^{\infty} \mathrm{d}z V(z) < 0$, ensure the existence of a value ℓ_0 which minimizes the function $E(\ell)$. We emphasize that ℓ_0 depends, of course, on the potential, and is attained in integral (27) only for values of x such that $|x| < \ell_0$. Assuming that the second derivative of E is well defined at ℓ_0, we can apply the saddle point method for $|x| < \ell_0$. This provides the general result

$$\rho_{\mathrm{erg}}(x,x,\beta) \overset{\beta\to\infty}{\sim} n(x)\Gamma(\beta) \tag{30}$$

for $|x| < \ell_0$. In (30), $n(x)$ is the unnormalized density

$$n(x) = \frac{1}{\ell_0}\sin^2\left[\frac{\pi(x+\ell_0)}{2\ell_0}\right](\exp[-\varphi^+(\ell_0, x/\ell_0)] + \exp[-\varphi^-(\ell_0, -x/\ell_0)]), \tag{31}$$

while the temperature dependence is entirely embedded into

$$\Gamma(\beta) = \frac{\pi^2\lambda_D}{8\ell_0}\sqrt{\frac{2\pi\hbar^2}{m\ell_0^4 E''(\ell_0)}}\exp[-\beta E(\ell_0)]. \tag{32}$$

We stress that temperature and position dependencies are factorized in formula (30), like in the exact low-temperature behavior (5). Although the temperature dependence of the ergodic density matrix is not entirely correct (because of the presence of factor λ_D in $\Gamma(\beta)$), the quantity $E(\ell_0)$ can be identified as the ergodic groundstate energy: indeed, it controls the exponential decay of $\rho_{\mathrm{erg}}(x,x,\beta)$ when $\beta \to \infty$. Below, we show, through several examples, that $E(\ell_0)$ is a good approximation for the real groundstate energy.

For $|x| > \ell_0$, the saddle point ℓ_0 is outside the integration range of (27). In that case, $\rho_{\mathrm{erg}}(x,x,\beta)$ could be evaluated by expanding the involved integrand for ℓ close to $|x|$. Of course, for a given β, if x becomes sufficiently large, $\rho_{\mathrm{erg}}(x,x,\beta)$ tends to the classical Boltzmann factor which, by the way, vanishes exponentially fast.

Now, we turn to specific forms of $V(x)$. First, let us consider confining potentials $V(z) = a_n z^n/n$, where n is an even integer and $a_n > 0$. The associated Schrödinger equation depends only on the two parameters $\hbar^2/m$ and a_n. Only one typical energy $\varepsilon_p = (\hbar^2/m)^{n/(n+2)} a_n^{2/(n+2)}$ and one typical length $\ell_p = [\hbar^2/(ma_n)]^{1/(n+2)}$ can be built in terms

of those parameters. Therefore, the energy and the spatial extension of the ground state are proportional to those typical energy and length respectively. Formula (30) can be used to compute the ergodic density matrix elements in the low temperature regime for $|x| < \ell_0$. Function $E(\ell)$ reads

$$E(\ell) = \frac{\pi^2\hbar^2}{8m\ell^2} + \frac{a_n \ell^n}{n} R_n, \tag{33}$$

where $R_n = \int_{-1}^{1} \mathrm{d}z \cos^2(\pi z/2) z^n$ is a pure numerical coefficient. The minimum of above expression, reached for $\ell_0 = \ell_p(\pi^2/4R_n)^{1/(n+2)}$, is

$$E(\ell_0) = a_n \ell_0^{\,n} R_n \left[\frac{1}{2} + \frac{1}{n}\right]. \tag{34}$$

We also find

$$\begin{aligned}\varphi^{\pm}(\ell_0, x/\ell_0) = {} & \frac{\pi}{2nR_n}\left[2\int_0^1 \mathrm{d}z \sin(\pi z) z^{n+1} - \int_{x/\ell_0}^1 \mathrm{d}z \sin(\pi z) z^n\right] \\ & + \frac{\pi}{2nR_n}\left(\frac{x}{\ell_0}\right)\tan\left(\frac{\pi x}{2\ell_0}\right) \\ & \times \left[\int_0^1 \mathrm{d}z \cos^2\left(\frac{\pi z}{2}\right) z^n - \frac{\ell_0}{x}\int_0^{x/\ell_0} \mathrm{d}z \cos^2\left(\frac{\pi z}{2}\right) z^n\right]\end{aligned} \tag{35}$$

which provides $n(x)$. Two important comments are in order. The scaling properties of the groundstate energy and extension are indeed recovered within the ergodic approximation. Table 1 presents a comparison with the numerical resolution of Schrödinger equation. The agreement, already good for low values of the exponent n, becomes better when n increases. This could be expected *a priori*, because the ergodic approximation becomes exact for an infinite square well potential. Comparisons for the groundstate pdf are presented in Fig. 7: the agreement is impressive.

Second, we consider a modified Pöschl–Teller potential namely $V(x) = -V_0/[\sqrt{2}\cosh(x/l_p)]^2$ with $V_0 > 0$. The spectrum of the corresponding Hamiltonian is exactly known. In particular, the groundstate energy is given by $E_0 = -(V_0/2)(\sqrt{1+2\gamma/\pi^2} - \sqrt{2\gamma}/\pi)^2$ with $\gamma = \pi^2\hbar^2/(8ml_p^2V_0)$. Parameter γ^{-1} controls the strength of the confinement: for γ^{-1} sufficiently small, the groundstate is the sole bound state, while the number of bound states increases when γ^{-1} increases. Now, the ergodic energy reads

$$E(\ell_0) = V_0\left(\gamma\left(\frac{l_p}{\ell_0}\right)^2 - \int_0^1 \mathrm{d}z \frac{\cos^2(\pi z/2)}{\cosh^2(z\ell_0/l_p)}\right), \tag{36}$$

Table 1 Comparison of the ergodic groundstate energy $E(\ell_0)$ derived by using formula (34), to the exact result E_0 (obtained by numerically solving Schrödinger equation). Integer n is the exponent of the anharmonic potential

n	2	4	6	8	10
$\frac{E(\ell_0)-E_0}{E_0}$	13%	12%	10%	7.5%	6%

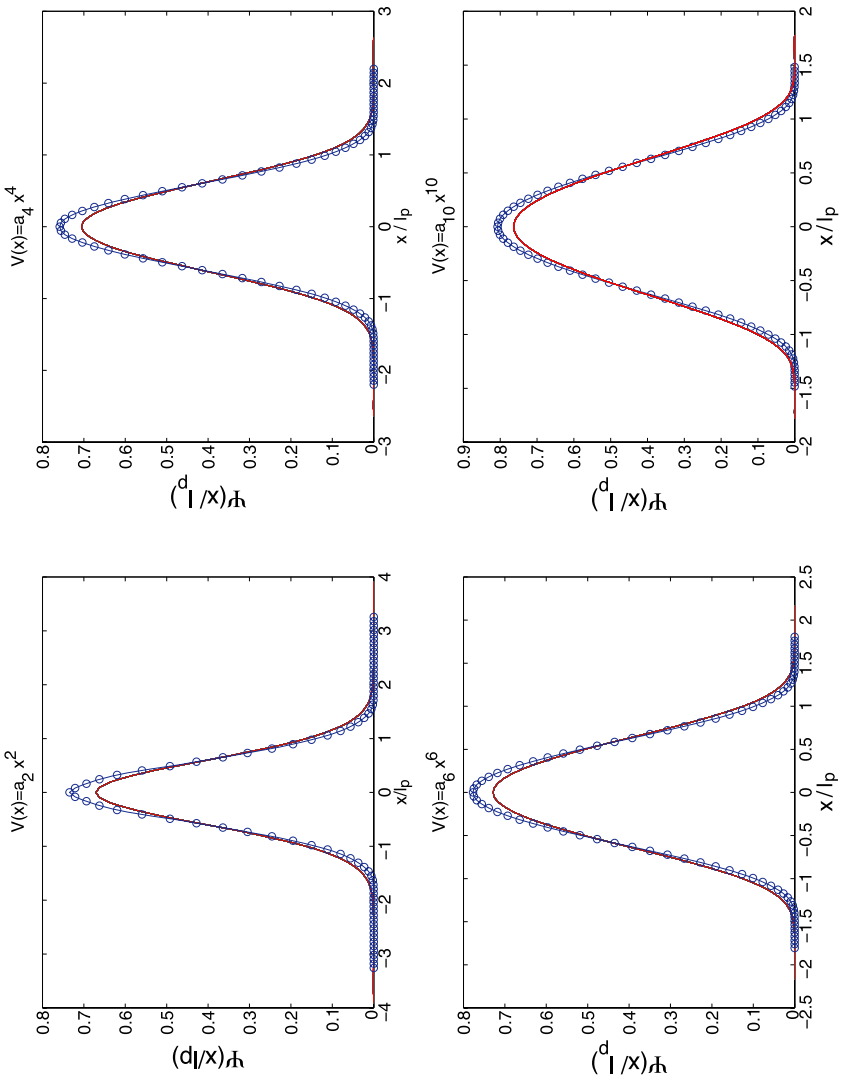

Fig. 7 (Color online) Probability density function of the ground state for confining potentials. The solid line is obtained through a numerical resolution of Schrödinger equation, while points correspond to the ergodic approximation obtained from (35)

Table 2 Comparison of the ergodic groundstate energy $E(\ell_0)$ derived by using formula (36), to the exact result E_0

γ	0.01	0.1	1	5	10
$\frac{E(\ell_0)-E_0}{E_0}$	1.33%	4.8%	20%	43%	50%

where ℓ_0 is the unique solution of

$$\gamma\left(\frac{l_p}{\ell_0}\right)^3 = \int_0^1 \mathrm{d}z \frac{\cos^2(\pi z/2)\tanh(z\ell_0/l_p)}{\cosh^2(z\ell_0/l_p)}. \tag{37}$$

In Table 2 we compare $E(\ell_0)$ to E_0 for different values of γ. Figure 8 shows the corresponding comparisons for the groundstate pdf's. For values of γ smaller than 1, ergodic energies stay close to the exact values and ergodic groundstate pdf's are quite good. Even for values of γ of order 1, the main shape of the groundstate pdf remains well approximated. If we set $\gamma \to \infty$ by taking the double limit $l_p \to 0$ and $V_0 \to \infty$ with $V_0 l_p = C$ fixed, then $V(x)$ reduces to the singular potential $-C\delta(x)$. In that rather unfavorable case, the discrepancy between $E(\ell_0)$ and E_0 becomes of order 60 percent. However, notice that the ergodic approximation does predict the existence of a bound state, contrarily to semi-classical estimations.

From the low-temperature behavior of the semi-classical density matrix [11], we extract the semi-classical groundstate energy $E_{\mathrm{sc}} = V(0) + \hbar\omega_0/2$ with $\omega_0 = [\mathrm{d}^2V/\mathrm{d}x^2(0)/m]^{1/2}$. That simple formula can be interpreted by noticing that the semi-classical approximation then amounts to replace the genuine potential by its harmonic local form near its minimum at $x = 0$. For considered anharmonic potentials, E_{sc} vanishes because $\omega_0 = 0$, so the semi-classical approximation completely fails at low temperatures. For the modified Pöschl–Teller potential, E_{sc} becomes exact when the confinement is strong, i.e. when $\gamma \to 0$, in agreement with the fact that the semi-classical approximation turns to be exact for a harmonic potential. Above a given value of γ, E_{sc} becomes positive so the semi-classical approximation erroneously predicts that all bound states disappear.

5.2 Intermediate and High Temperature Regimes

At intermediate temperatures, formula (21) is implemented through simple numerical evaluations of ordinary integrals. As shown below, the ergodic approximation is particularly efficient in that regime or, in other words, it provides a good interpolation between the exact behaviors at high and low temperatures. Here, we consider both global and local quantities, namely internal energy $U = -\partial_\beta(\log(Z(\beta))$ and probability density function (PDF) $\Psi(x,\beta) = \rho(x,x,\beta)/Z(\beta)$ for confining potentials ($V(x) \to \infty$) on the one hand, virial coefficient $B(\beta)$ and deviation $\Phi(x,\beta) = [\rho(x,x,\beta) - (\sqrt{2\pi}\lambda_D)^{-1}]/B(\beta)$ for hole potentials ($V(x) \to 0^-$) on the other hand. Comparisons are made with either numerically exact results or other familiar approximations.

The ergodic approximation appears to be rather accurate for estimating the considered thermodynamic quantities. There always exists a large-temperature domain where the ergodic approximation is significantly better than other considered approximations. Above temperature domain becomes larger when the anharmonicity of the potential increases. Figures 9 and 10 show results for respectively, the anharmonic potential $V(x) = a_4x^4$, and the modified Pöschl–Teller potential with $\gamma = 1$.

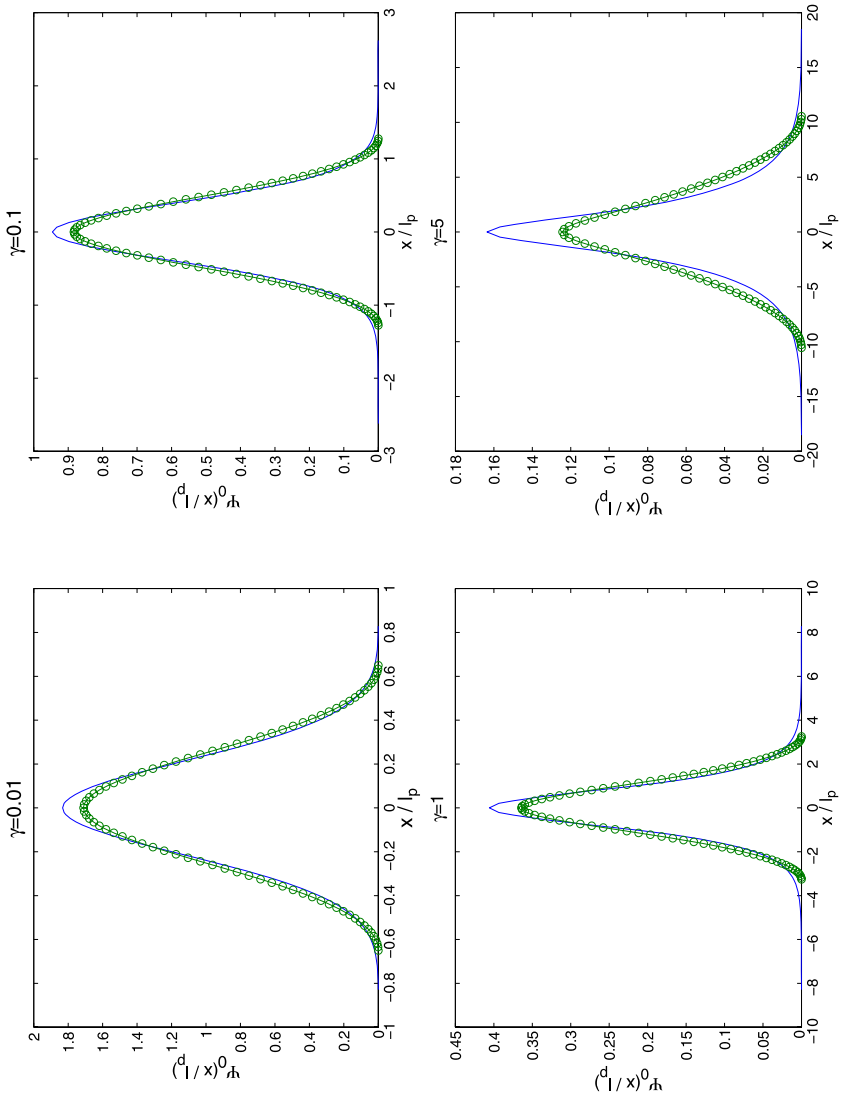

Fig. 8 (Color online) Probability density function of the ground state for modified Pöschl–Teller potential. The solid lines represent the exact ground states pdf, while points correspond to their ergodic approximation

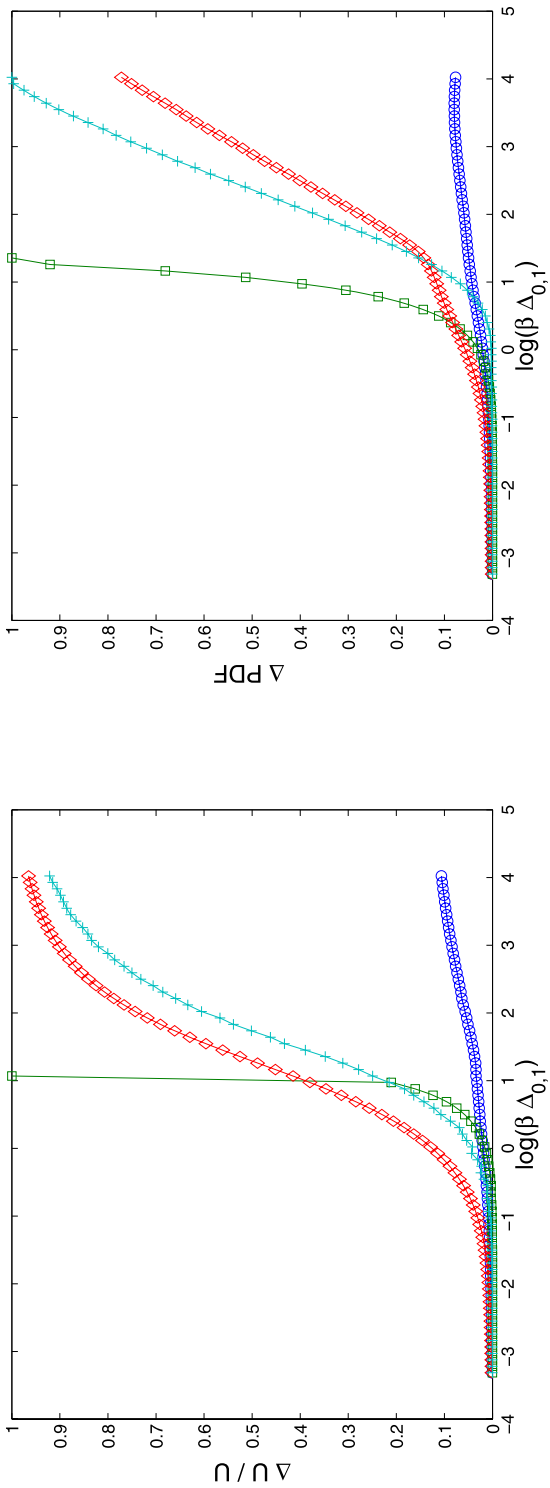

Fig. 9 (Color online) Relative error for internal energy (*left panel*) and mean-square error for the probability density function Ψ (*right panel*), as functions of the temperature for the potential $V(x) = a_4 x^4$. *Circles* correspond to the ergodic approximation, *squares* refer to Wigner–Kirkwood expansion truncated up to order $\hbar^2$, *crosses* describe the semi-classical approximation and diamonds are the classical values. Quantity $\Delta_{0,1}$ is the energy gap between the ground state and the first excited one

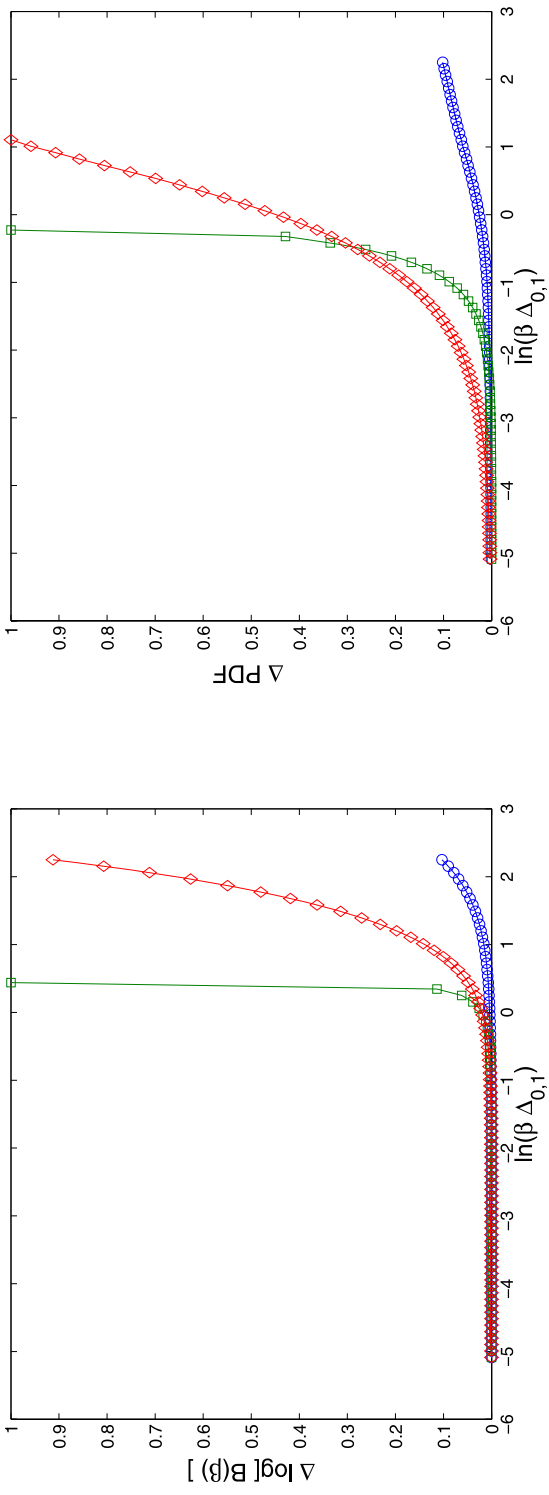

Fig. 10 (Color online) Relative error for virial coefficient (*left panel*) and mean-square error for the probability density function Φ (*right panel*), as functions of the temperature for the $\gamma = 1$ modified Pöschl–Teller potential. *Circles* correspond to the ergodic approximation, *squares* refer to Wigner–Kirkwood expansion truncated up to order $\hbar^2$ and *diamonds* are the classical values. Quantity $\Delta_{0,1}$ is the energy gap between the ground state and the first excited one

Either the Wigner–Kirkwood expansion or the semi-classical approximation become well-suited when the temperature increases. Does the ergodic approximation provides satisfactory results in the high temperature regime? More precisely, what part of the Wigner–Kirkwood expansion is accounted for within that approximation? We obtain, in that regime,

$$\rho_{\rm erg}(x,x,\beta) \overset{\beta\to 0}{\sim} \frac{e^{-\beta V(x)}}{\sqrt{2\pi}\lambda_D}\left[1-\beta\frac{{\rm d}^2V}{{\rm d}x^2}\frac{\lambda_D^2}{12}+\left(\beta\frac{{\rm d}V}{{\rm d}x}\right)^2\frac{\lambda_D^2}{24}A_0+o(\lambda_D^2)\right], \tag{38}$$

with the pure numerical coefficient

$$\begin{aligned} A_0 = &-\frac{1}{2}+3\sqrt{2\pi}\int_0^1 {\rm d}s\left(\frac{s}{1-s}\right)^{3/2} \\ &\times\int_0^\infty {\rm d}z z^2\,{\rm erfc}^2\left(\frac{z}{\sqrt{2s}}\right)\exp\left(-\frac{z^2(2s-1)}{2s(1-s)}\right) \\ &+3\sqrt{2\pi}\int_0^1 {\rm d}s\int_0^\infty {\rm d}z z^2\,{\rm erfc}\left(\frac{z}{\sqrt{2s}}\right){\rm erfc}\left(\frac{z}{\sqrt{2(1-s)}}\right)\simeq 0.8. \end{aligned} \tag{39}$$

Thus, the ergodic approximation does provide the leading classical term, while part of the $\hbar^2$-correction is also correctly reproduced. At that order $\hbar^2$, the discrepancy of (38) with exact expansion (4), arises from correlations between occupation times which are not taken into account in the ergodic approximation. Moreover, A_0 is indeed smaller than 1 in agreement with inequality $\rho_{\rm erg}(x,x,\beta)\le\rho(x,x,\beta)$. Eventually, the ergodic approximation turns out to be also quite reasonable at high temperatures.

5.3 Further Applications and Extensions

For a single particle, the ergodic approximation can been also applied to other one-dimensional potentials of interest (Morse, double well, periodic, ...), with possible simple modifications of box formula (13). For instance, for asymmetric Morse potential defined for $x>0$ ($V(x)=\infty$ for $x<0$), the confining box is chosen as $[0,\ell]$ of course. According to preliminary calculations, accuracy of the ergodic approximation is comparable to that observed above.

The extension of the ergodic approximation to two- or three-dimensional potentials requires the derivation of suitable box formulas similar to (13). A first possible route starts with an auxiliary Hamiltonian which tends to confine the particle inside a disk or a sphere with radius ℓ. This provides an exact formula identical to (13), except for an additional ordinary integral over the angle(s) of the boundary touching point. The corresponding ergodic approximation involves an occupation-time average, which is easily expressed in terms of the known free Green functions with Dirichlet boundary conditions on a disk or on a sphere.

For two particles with an interaction potential $V(\mathbf{r}_1,\mathbf{r}_2)=V(\mathbf{r}_1-\mathbf{r}_2)$ which depends only on their relative position $\mathbf{r}_1-\mathbf{r}_2$, thanks to the trivial motion of their mass center we are left with the previous case of a single particle in an external potential $V(\mathbf{r})$. For other cases, like two interacting particles in an external potential or three interacting particles, box formulas could also be derived in the same spirit as (13). Nevertheless, the corresponding ergodic approximation should become rather difficult to numerically handle because of the increasing number of intricated ordinary integrals.

Appendix Statistical weights of boxes

Eigenstates and eigenvalues of the auxiliary Hamiltonian H_ℓ^0 are obtained by solving the Schrödinger equation

$$\frac{\mathrm{d}^2\phi_\ell^0}{\mathrm{d}z^2} = \frac{2mV_0}{\hbar^2}\left[1 - \Theta(z+\ell) + \Theta(z-\ell) - \frac{E}{V_0}\right]\phi_\ell^0(z). \tag{40}$$

After introducing dimensionless function $\psi(z) = \sqrt{\ell}\phi_\ell^0(z)$ and setting $E_n = \pi^2\hbar^2 n^2/(8m\ell^2) = E_1 n^2$ for the n-th eigenvalue in the large-V_0-limit, a straightforward calculation leads to

$$\psi_n(z^\ell) \overset{V_0\to\infty}{\sim} \begin{cases} \sqrt{\frac{E_1}{V_0}}n, & \text{if } z = -\ell, \\ \sin\left[\frac{n\pi}{2\ell}(z+\ell)\right], & \forall z \in]-\ell, +\ell[, \\ (-1)^{(n-1)}\sqrt{\frac{E_1}{V_0}}n, & \text{if } z = \ell. \end{cases} \tag{41}$$

By using spectral decomposition (1), we eventually obtain the following expression for the statistical weight functions

$$g\pm(x,\ell,s,\beta) = \sqrt{2\pi}\frac{\pi^2\lambda_D^3}{8\ell^4} S_g^\pm\left(\frac{x}{\ell}, \frac{\pi\lambda_D\sqrt{s}}{2\ell}\right) S_g^\pm\left(\frac{x}{\ell}, \frac{\pi\lambda_D\sqrt{1-s}}{2\ell}\right), \tag{42}$$

where

$$S_g^\pm(\alpha, y) = \sum_{n=1}^{\infty} n(\mp 1)^{n-1} \sin\left[n\frac{\pi}{2}(\alpha+1)\right]\exp\left[-\frac{y^2}{2}n^2\right]. \tag{43}$$

Those two functions satisfy the equality $g^+(x,\ell,s,\beta) = g^-(-x,\ell,s,\beta)$, the normalization condition

$$\int_{|x|}^{\infty}\mathrm{d}\ell\int_0^1 \mathrm{d}s[g^-(x,\ell,s,\beta) + g^+(x,\ell,s,\beta)] = 1, \tag{44}$$

and their asymptotic form merely is

$$g\pm(x,\ell,s,\beta) \overset{\lambda_D\gg\ell}{\sim} \sqrt{2\pi}\frac{\pi^2\lambda_D^3}{8\ell^4}\sin^2\left[\frac{\pi(x+\ell)}{2\ell}\right]\exp\left[-\frac{\pi^2\lambda_D^2}{8\ell^2}\right] \tag{45}$$

in the low temperature regime. The asymptotic expression of $g\pm$ in the high-temperature regime is derived from the Poisson transform of expression (43). According to Poisson formula, if the Fourier transform of a function f exists, then, for all values of Δy

$$\Delta y\sum_{n=-\infty}^{\infty} f(n\Delta y) = \sum_{m=-\infty}^{+\infty}\int_{-\infty}^{+\infty}\mathrm{d}z f(z)\, e^{-\mathrm{i}m2\pi z/\Delta y}. \tag{46}$$

Application of that transformation to expression (43) provides

$$\begin{aligned} g^-(x,\ell,s,\beta) &= g^+(-x,\ell,s,\beta) \\ &\overset{\lambda_D\ll\ell}{\sim} \sqrt{\frac{2}{\pi}}\frac{\ell^2}{\lambda_D^3}\frac{1}{\sqrt{s(1-s)}}\frac{(1+x/\ell)^2}{s(1-s)}\exp\left[-\frac{\ell^2}{2\lambda_D^2}\frac{(1+x/\ell)^2}{s(1-s)}\right] \end{aligned} \tag{47}$$

in the high temperature regime.

References

1. Feynman, R.P., Hibbs, A.R.: Quantum Mechanics and Path Integrals. McGraw–Hill, New York (1965)
2. Simon, B.: Functional Integration and Quantum Physics. Academic, New York (1979)
3. Schulman, L.S.: Techniques and Applications of Path Integrals. Wiley, New York (1981)
4. Roepstorff, G.: Path Integral Approach to Quantum Physics. Springer, Berlin (1994)
5. Kleinert, H.: Path Integrals in Quantum Mechanics, Statistics, and Polymer Physics, and Financial Markets. World Scientific, Singapore (2004)
6. Wigner, E.P.: Phys. Rev. **40**, 749 (1932)
7. Kirkwood, J.G.: Phys. Rev. **44**, 31 (1933).
8. Kirkwood, J.G.: Phys. Rev. **45**, 116 (1934)
9. Landau, L., Lifschitz, E.: Statistical Physics. Pergamon, Elmsford (1980)
10. Feynman, R., Kleinert, H.: Phys. Rev. A **34**, 5080 (1986)
11. Dashen, R., Hasslacher, B., Neveu, A.: Phys. Rev. D **10**, 4114 (1974)
12. Bogojeviè, A., Balaž, A., Beliè, A.: Phys. Lett. A **345**, 258 (2005)
13. Raffarin, J.P.: General communication (2004)
14. Bogojeviè, A., Balaž, A., Beliè, A.: Phys. Lett. A **344**, 84 (2005)
15. Krauth, W.: Introduction to Monte Carlo algorithms. In: Kertesz, J., Kondor, I. (eds.) Advances in Computer Simulation. Lecture Notes in Physics. Springer, Berlin (1998)
16. Krauth, W.: Statistical Mechanics: Algorithms and Computations. Oxford University Press, Oxford (2006)
17. Ceperley, D.M.: Rev. Mod. Phys. **67**, 279 (1995)
18. Militzer, B., Ceperley, D.M.: Phys. Rev. E **63**, 066404 (2001)
19. Predescu, C., Sabo, D., Doll, J.D.: J. Chem. Phys. **119**, 4641 (2003)
20. Ginibre, J.: Some applications of functional integration in statistical mechanics. In: DeWitt, C., Stora, R. (eds.) Statistical Mechanics and Quantum Field Theory. Gordon and Breach, Les Houches (1971)
21. Cornu, F.: Phys. Rev. E **53**, 4562 (1996)
22. Brydges, D.C., Martin, Ph.A.: J. Stat. Phys. **96**, 1163 (1999)
23. Martin, Ph.A.: Acta Phys. Pol. B **34**, 3629 (2003)
24. Kihara, T., Midzuno, Y., Shizume, T.: J. Phys. Soc. Jpn. **10**, 249 (1955)
25. Gradshteyn, I.S., Ryzhik, I.M.: Tables of Integrals Series and Products, 5th edn. Academic Press, New York (2000)